Applications of NMR based methodologies investigating the behavior of lignin and cellulose towards bio-based carbon fibers production

Solid State Nuclear Magnetic Resonance 134 (2024) 101977

Contents lists available at ScienceDirect

Solid State Nuclear Magnetic Resonance

journal homepage: www.elsevier.com/locate/ssnmr

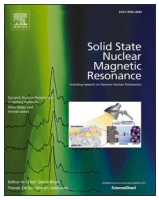

Applications of NMR based methodologies investigating the behavior of lignin and cellulose towards bio-based carbon fibers production

Feryal Guerroudj [a], Lukas Fliri [b], Jenny Bengtsson [c], Leandro Cid Gomes [a], Tristan Gazzola [a], Michael Hummel [b], Diana Bernin [a,*]

[a] Chalmers University of Technology, Gothenburg, Sweden
[b] Aalto University, Aalto, Finland
[c] RISE Research Institutes of Sweden, Mölndal, Sweden

ARTICLE INFO

Handling Editor: Prof D Bryce

Keywords:
Thermostabilization
Pyrolysis
Coagulation
Fractionation
Heat treatment
Thermal conversion
Bio-based polymers

ABSTRACT

Cellulose–lignin blends are proposed as alternative precursors for carbon fiber (CF) production, offering a potential sustainable and cost-effective alternative to the expensive fossil-based polymers currently used. The characteristics of the precursor fibers including their crystallinity, the incorporated chemical structures and the distribution of the biopolymers have a significant influence on their carbonization behavior and the properties of the CFs. They are partly determined by the composition of the bio-based resources and the conditions used during the fiber fixation, i.e. the coagulation, an important processing step. In this work, ^{13}C solid and 2D solution NMR methodologies were applied to investigate the impact of coagulation and thermostabilization conditions on cellulose and cellulose-lignin blends using a thin film model. Solid state NMR spectroscopy showed that the choice of the anti-solvent influenced the proportion of cellulose II *versus* amorphous regions in the coagulated films. Independent of the presence of lignin, the choice of anti-solvent seems to impact the rate of thermal reactions. After thermostabilization at 245 °C, the samples were investigated using a solution NMR protocol devised for cellulosic materials. At 275 °C, most of the samples became insoluble for solution NMR. However, solid state NMR revealed further changes in the chemical composition, which were dependent on both the presence of lignin and the choice of anti-solvent. This multi-faceted approach combining solid state and 2D solution NMR techniques provides a comprehensive understanding of the cellulose structure and the products formed for cellulose-lignin-based CFs, which is crucial for optimizing their properties and potential applications.

1. Introduction

The society is facing multiple challenges *e.g.*, climate catastrophes due to an increased level of CO_2 in the atmosphere [1], pollution of oceans and depletion of resources, caused by the unsustainable use of plastics in particular from fossil-based resources [2]. One way forward is substituting fossil-based compounds with renewable and bio-based counterparts [3,4]. Electrification of the transport sector is another crucial step which requires light weight construction for a longer battery time [5].

Carbon fibers (CFs) show desirable weight-to-strength ratios as they have a high specific strength and stiffness, which makes them very efficient reinforcements in light weight composite materials. Since the 1970s, the growing market of carbon fibers has been dominated by CFs made from fossil-based precursor fibers, predominantly prepared from polyacrylonitrile. This process was optimized and CFs with exceptional mechanical properties can be prepared on an industrial scale. However, due to the high cost of the precursor comprising approximately 50 % of the total cost of the CFs [6], applications are effectively restricted to higher end industries. To enter lower end industries like the automotive or construction sectors cheaper CFs are needed [7].

Besides cost considerations, a shift towards forest-based products as precursors for carbon fibers aligns with the growing emphasis on sustainability and the need to reduce dependency on fossil resources. Recent research showed that bio-based resources such as lignin and cellulose could potentially replace fossil-based ones for CFs production [6,8,9].

Both these bio-based materials have been investigated separately for the production of CFs and both suffer from intrinsic drawbacks. Cellulose carbonization usually results in low char yield (10–30 % at

* Corresponding author.
E-mail address: diana.bernin@chalmers.se (D. Bernin).

https://doi.org/10.1016/j.ssnmr.2024.101977
Received 29 July 2024; Received in revised form 19 November 2024; Accepted 20 November 2024
Available online 21 November 2024

1000 °C). To remove incorporated oxygen containing moieties and enhance the mechanical strength, hot stretching is required [10]. On the other hand, lignin-based CFs require a long stabilization time to prevent fiber fusion, which makes it impractical for industrial production [11,12]. Through carbonization of cellulose-lignin blends these issues can be partially addressed [13–17].

Different methods have been developed to prepare bio-based precursor fibers. For instance, melt [18], dry [19] and wet-spinning [13,14,16,17,20,21] techniques were proposed. In recent research air-gap spinning of cellulose-lignin blends was put forward as a very promising method [22]. It allows the cellulose chains to be highly aligned in the fibers [23,24]. In this method, cellulose and lignin are first dissolved in for example an ionic liquid [15,25] or *N*-methylmorpholine *N*-oxide (NMMO) monohydrate [26]. The cellulose-lignin blends are then extruded through a coagulation bath containing an anti-solvent (such as water) and spun into continuous fibers. Further steps include thermostabilization (heating up to 300 °C under air atmosphere) and carbonization (heating up to 1000 °C and beyond under nitrogen flow) of the spun fibers for the conversion into CFs. Successful conversion of cellulose-lignin precursor fibers to carbon fibers, on a lab scale, was reported with tensile strengths reaching up to 1070 MPa [20,27]. However, the so far achieved mechanical properties of cellulose-lignin CFs do not meet the requirements even for lower performance applications yet [7]. Another important factor in CF production is the obtainable char yield. The yield of bio-based CFs prepared from air-gap spun precursors can be increased by increasing the lignin to cellulose ratio [15,17]. However, technical lignins are very complex polymers with multiple functional groups and broad molecular weight distributions. Subsequently, depending on the anti-solvent used during coagulation, some of the added lignin might remain dissolved in the coagulation bath [28].

Furthermore, it is also well known that coagulation causes formation of cellulose II with varying total crystallinity [29,30]. For example, Cao et al., 2014 [29] showed that after the coagulation of microcrystalline cellulose dissolved in the ionic liquid 1-butyl-3-methylimidazolium chloride, mainly amorphous cellulose was obtained when using acetone as anti-solvent, while cellulose II was found when coagulating in water and ethanol. Moreover, the exceptional thermal stability of cellulose is believed to be a consequence of the crystalline regions. Thus, having a higher share of amorphous cellulose in the precursors may impact the thermostabilization [31].

In cellulose research, ^{13}C solid state NMR using cross-polarization (CP) and magic-angle spinning (MAS), is a tool for observing the polymorphs and the crystallinity [32–35] and delineating the characteristic features of cellulose [35–38]. ^{13}C CP MAS NMR is typically used to enhance the signal intensity of carbon resonances, by a magnetization transfer from the ^{1}H directly attached or in close vicinity. It allows then to distinguish between crystalline and amorphous cellulose by observing differences in chemical shifts and line widths, which arise due to differences in local environments and molecular motions. Crystalline regions of cellulose exhibit well-defined chemical shifts in the NMR spectrum, while amorphous regions typically show broader signals due to a range of local environments and dynamics [39].

Solid state ^{13}C NMR was also extensively used to investigate the changes in thermally treated celluloses. Both supramolecular changes [40] and further carbonization reactions could be followed [41–43]. More detailed insights in the formed structures could be obtained by 2D solid state ^{1}H-^{13}C HETCOR experiments [44]. However, a 2D solid state NMR spectrum may improve the resolution for cellulose-based components, but this depends on the concentration of the products and the heterogeneity of the sample but will nevertheless require long experimental times. Moreover, standard solid state NMR methods like one-dimensional ^{13}C CP MAS may only give limited information on the chemical transformations occurring up to 250 °C due to insufficient spectral resolution [41]. Recent studies attempted to overcome these inherent limitations by applying a solution NMR protocol to thermally treated cellulosic materials [45,46], through dissolution of the cellulose samples in an NMR electrolyte consisting of tetra-*n*-butylphosphonium acetate [P_{4444}][OAc] diluted with DMSO-d_6 (1:4 wt%). Applying this protocol allowed further insights into the transformations of the polysaccharide. The 2D solution NMR spectra showed that the main chemical transformation below 250 °C was the formation of levoglucosan end capped moieties. However, after prolonged heat treatment the formation of an insoluble thermostable condensed phase prevented further insights in the dehydration reactions [41,47]. Therefore, a combination of solid state and solution NMR could be a promising approach to overcome the persisting sensitivity and solubility issues of the independent techniques.

Solid state ^{13}C CP MAS NMR is especially useful for analyzing crystallinity and amorphous structures, while solution NMR excels at capturing the chemistry and reactions occurring at lower thermostabilization temperatures. For harsher thermostabilization conditions, solid state NMR could be again more useful, provided that spectral resolution is enhanced. This may be achieved with spectral deconvolution or if there would be differences in ^{13}C T_1 relaxation times [48–51]. Solid state dynamic nuclear polarization (DNP) NMR could offer a higher signal-to-noise ratio but requires sample preparation for optimal radical penetration. Nevertheless, DNP NMR provided deeper insights into the surface chemistry and structure of cellulose [52], using ^{13}C-unlabeled [53] or labeled materials [54,55].

Other techniques including Wide Angle X-ray Scattering, Raman spectroscopy [56,57], infra-red spectroscopy, and X-ray photoelectron spectroscopy [58,59], have been used to investigate biomaterials, providing qualitative or semi-quantitative information. However, these techniques provide less details in terms of functional groups, linkages, and chemical environments compared to solid state and solution NMR spectroscopy. Moreover, some of the listed techniques such as synchrotron-based measurements, are challenging to implement, and require expensive infrastructure and extensive expertise to be applied successfully.

As lignin can be solubilized in common perdeuterated solvents, studies have focused on solution NMR techniques [60–62]. On the other hand, lignin's solid state NMR spectrum is rather featureless, due to its complexity, number of functional groups and molecular weight distributions. For cellulose-lignin blends, solution NMR protocols developed for lignin cannot easily be adapted due to solubility issues of the cellulosic fractions. Hence the solution NMR methodology described earlier was applied to get further insights in the thermal reactions of cellulose-lignin blends [63].

Here we investigated the behavior of lignin and cellulose during the different processes, coagulation and thermostabilization relevant to bio-based carbon fiber production. We used two different anti-solvents, water and ethanol, and two different molecular weight fractions of a technical softwood Kraft lignin. Induced changes in cellulose and lignin were monitored using ^{13}C solid state and ^{1}H-^{13}C solution NMR. We further discuss the advantages and disadvantages with the different NMR based methodologies for bio-based carbon fiber production based on lignin and cellulose. Understanding the behavior of cellulose and lignin, as well as the synergies that occur during the different stages of the process, such as coagulation and thermostabilization, is crucial for optimizing cellulose-lignin based CFs production and enhancing their performance.

2. Experimental

2.1. Materials

Softwood Kraft dissolving grade pulp (Buckeye v67) purchased from Georgia Pacific (Atlanta, GA) was used as a cellulose source. The intrinsic viscosity was 465 ml/g according to ISO 5351. Softwood Kraft lignin was received from Bäckhammar Pilot Plant (Bäckhammar, Sweden). It was isolated with the LignoBoost method using industrial black

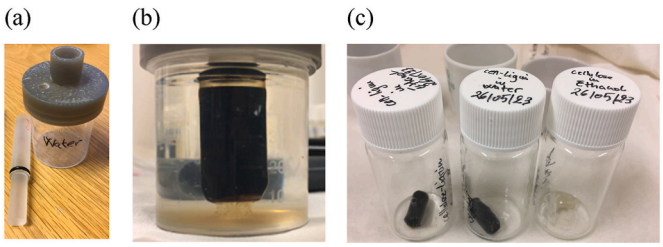

Fig. 1. Model setup for filament coagulation (a). A cellulose-lignin film during the coagulation process (b). Washed, dried and thermostabilized cellulose-lignin films (c).

liquor. The Kraft lignin was fractionated into high molecular weight (HMW) and low molecular weight (LMW) lignin. Acetone (USP ACS, VWR, Sweden) and hexane (98.5 %, Fisher, Sweden) were used as solvents in the fractionation of softwood Kraft lignin.

The ionic liquid 1-ethyl-3-methylimidazolium acetate ([EMIM]OAc, ≥98 %, Proionic) was used for cellulose and lignin dissolution and was used as received. The two anti-solvents were ethanol (95 %, Aldrich) and deionized water (MilliQ). The tetra-*n*-butyl phosphonium acetate [P_{4444}][OAc]:DMSO-d_6 (1:4 wt%) electrolyte was prepared according to literature [63] and used as a solvent for the solution NMR measurements. Dimethyl sulfoxide, DMSO, (HPLC grade, >99.7 %) and lithium bromide, LiBr, (>99 %) were purchased from Sigma Aldrich and used for size exclusion chromatography (SEC) analysis.

2.2. Lignin fractionation by solvent-assisted precipitation

The softwood Kraft lignin was fractioned following the procedure by Cui et al. [64]. In short, 80 g of softwood Kraft lignin was mixed into 800 mL of acetone. The mixture was filtered, and the supernatant was brought to a volume of 1 L with acetone. Then, 250 mL of hexane was slowly added, precipitating the high molecular weight (HMW) lignin fraction, which was separated by filtration. Then 750 mL of hexane was added to the remaining supernatant, precipitating the low molecular weight (LMW) lignin fraction, also separated by filtration.

2.3. Cellulose and lignin dissolution

Prior to dissolution, the HMW and LMW lignin was sieved (0.5 mm). The cellulose pulp sheets were first chopped into smaller pieces and then ground to roughly 1 mm sized particles. The sieved HMW and LMW lignin was dried overnight (60 °C, 100 mbar) and the ground cellulose at 40 °C to reduce the water content. The solutions were prepared by adding an appropriate amount of cellulose (and lignin) to neat [EMIM]OAc at 70 °C which was stirred for 1 h in a closed reactor with overhead stirring at 30 rpm.

Solutions contained either 8 wt % (dry weight) of cellulose or a constant ratio of cellulose and lignin of 50:50 with a total concentration of 16 wt %.

2.4. Preparation of coagulated films using a model system

A model system for filament coagulation during wet spinning process was built based on a previous publication assuming that the mass transport of the solvents occurs radially [65]. This model setup was composed of a vial of 50 mL containing the anti-solvent and a piston mounted to the lid of the vial (Fig. 1a). A cylinder with a radius of 1 mm larger than the radius of the piston was filled with the [EMIM]OAc/-cellulose/lignin solution and the piston was pushed through the cylinder rendering a 1 mm thick film on the piston. Thereafter, the film covered piston was immersed in the anti-solvent (H_2O or EtOH) as illustrated in Fig. 1b. The obtained films, after 30 min of coagulation, were used as a model for precursor's fibers.

Table 1
Appearance of the solutions for solution NMR of the dissolved films coagulated in water (H_2O) or ethanol (EtOH). LMW refers to low molecular weight lignin and HMW to high molecular weight lignin.

Sample	Appearance
Cellulose in H_2O Cellulose in EtOH Cellulose LMW in H_2O Cellulose LMW in EtOH Cellulose HMW in H_2O Cellulose HMW in EtOH	Viscous solution without insoluble particles.
Cellulose in H_2O 245 °C Cellulose in EtOH 245 °C Cellulose LMW in H_2O 245 °C Cellulose LMW in EtOH 245 °C Cellulose HMW in H_2O 245 °C Cellulose HMW in EtOH 245 °C	Non-viscous solution, containing some small particles.
Cellulose in H_2O 275 °C Cellulose in EtOH 275 °C Cellulose LMW in H_2O 275 °C Cellulose LMW in EtOH 275 °C Cellulose HMW in H_2O 275 °C Cellulose HMW in EtOH 275 °C	Non-viscous solution, containing some bigger particles.

The films were washed with pure deionized water until conductivity measurements in the washing bath indicated a stabilized and low residual content of [EMIM]OAc. The films were subsequently dried in a vacuum oven overnight at 80 °C.

2.5. Thermostabilization of coagulated films

Two heating conditions were used for thermostabilization of the cellulose and cellulose-lignin films and a sample was taken for each: 245 °C for 30 min and 275 °C for 60 min, under air atmosphere, with a heating and cooling rate of 11 °C/min from ambient temperature then a cooling to 70 °C.

The washed and dried coagulated films (Fig. 1c) were crushed and first packed in 4 mm rotors for solid state NMR measurements. After the solid state NMR measurements, these films were dissolved (see 2.6) to perform solution NMR measurements.

2.6. Dissolution of the coagulated films for solution NMR characterization

For the dissolution of the coagulated films before and after thermostabilization a recently reported protocol using an electrolyte solution of tetra-*n*-butylphosphonium acetate [P_{4444}][OAc] diluted with DMSO-d_6 (1:4 wt%) was followed [63].

The films (25–50 mg) were weighed into a 4 mL glass vial, before [P_{4444}][OAc]:DMSO-d_6 (1:4 wt%) was added until a final weight of 1.0 g was achieved. The mixtures were stirred overnight with a small magnetic stirring bar at 65 °C. The solutions were transferred to 5 mm NMR tubes using short-necked Pasteur glass pipettes (150 mm, VWR).

As described in previous studies on thermostabilized Ioncell® fibers, heat treatment can result in partial or complete insolubility depending on the formation of a thermostabilized condensed phase [45,46]. Partially soluble samples were also encountered in this study (Table 1). Complete insolubility was observed for some samples treated at 275 °C.

2.7. Characterization methods

2.7.1. ^{13}C solid state NMR spectroscopy on coagulated films

^{13}C solid state NMR experiments were carried out on a Bruker Avance III 500 MHz spectrometer equipped with a 4 mm HX CP MAS probe. Cross-polarization (CP) experiments with a contact time of 1.5 ms

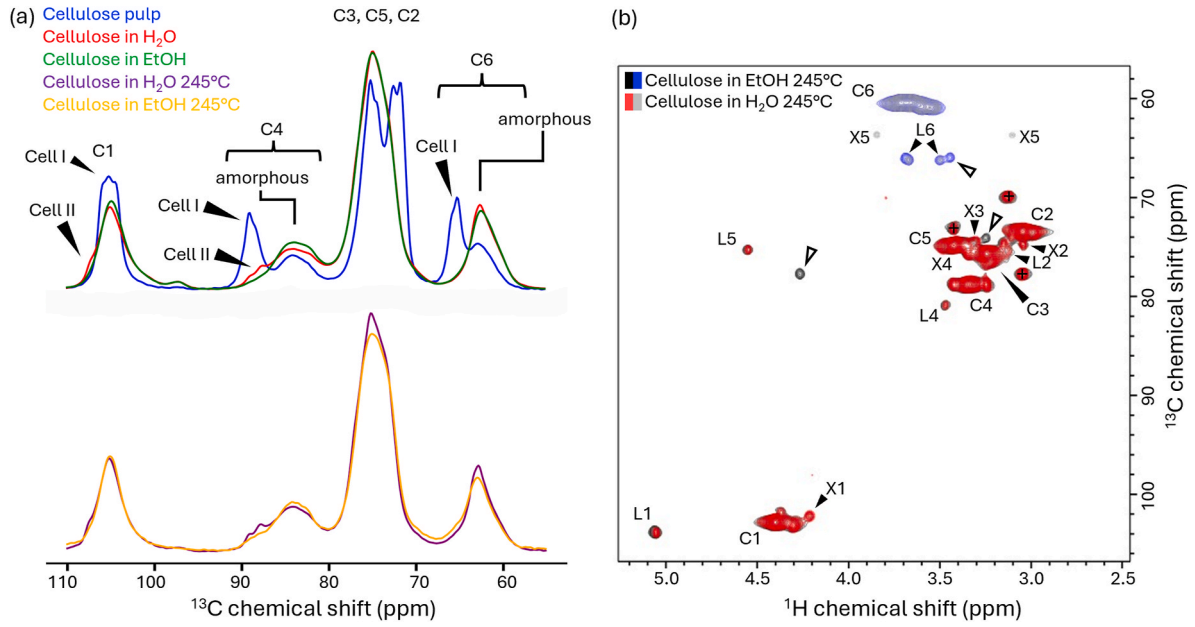

Fig. 2. (a) ^{13}C CP solid state NMR spectra of coagulated (EtOH and H_2O) cellulose films before and after thermostabilization at 245 °C. The spectra are normalized by their area. Cellulose pulp is the reference and starting material. (b) 2D ^{1}H-^{13}C HSQC spectra of the coagulated (EtOH and H_2O) cellulose films after thermostabilization at 245 °C. Open triangles identify unassigned peaks from unknown products and peaks marked with + are already present in the reference pulp. C refers to cellulose, X to xylan, L to levoglucosan end cap, Cell I to cellulose I and Cell II to cellulose II. The numbers refer to the atom number in the molecular structure. Blue and gray are CH_2 groups while black and red are CH or CH_3 groups. A summary of the chemical shifts is presented in Tables S1 and S2.

and a repetition time of 2 s were recorded at a magic angle spinning rate of 10 kHz. The temperature was set to 298 K. ^{1}H decoupling with a "spinal64" scheme at 77 kHz was applied during the acquisition [66]. The 90° radio frequency pulse duration was set to 4 μs and 3 μs for ^{1}H and ^{13}C respectively. The acquisition time was set to 13.6 ms and the spectral width to 596 ppm. The chemical shift scale was referenced using adamantane. All CP spectra were recorded with 4000 signal accumulations. The samples used for the measurements were dry without any ^{13}C labelling. The recorded spectra were processed on Topspin 4.2.0 and further processed and normalized with Python 3.12.

2.7.2. Solution NMR spectroscopy on dissolved coagulated films

The experiments were performed on a Bruker Avance III HD 700 equipped with a 5 mm QCI cryoprobe set to 65 °C. A multiplicity edited ^{1}H-^{13}C HSQC (hsqcedetgpsisp2.3) was recorded on the solutions according to the protocol [63]. The spectral widths were set to 20 and 200 ppm, with transmitter offsets of 6.2 and 75 ppm, for ^{1}H and ^{13}C dimensions, respectively. The relaxation delay was set to 1.5 s and 4 scans were accumulated. 512 points were recorded in the indirect dimension which was then zero-filled to 1024. DMSO-d_6 has been used as the lock solvent and hence as an internal standard. The recorded spectra were processed and analyzed with Topspin 4.2.0.

2.7.3. Size exclusion chromatography

The different molecular weight (MW) distributions of the fractionated lignin samples were estimated by size exclusion chromatography (PL-HPC 50 Plus Integrated GPC system, Polymer Laboratories, Varian Inc.). The system is equipped with two 300 × 7.5 mm PolarGel-M columns, one 50 × 7.5 mm PolarGel-M guard column, one refractive index (RI) detector and one ultraviolet (UV) detector operating at 280 nm. DMSO with 10 mM LiBr was used as the mobile phase and the flow rate was 0.5 mL/min at 50 °C. The RI detector was calibrated with 10 Pullulan standards ranging from 0.180 to 708 kDa (Varian PL2090-0100, Varian Inc), and the UV detector was calibrated based on the RI detector calibration. Lignin samples were prepared by dissolving ca. 10 mg in 1 mL of mobile phase under stirring overnight, then diluted to 0.25 mg/mL and filtered with 0.2 μm syringe filters. Film samples were prepared by leaching ca. 20 mg of the film in 1 mL of mobile phase under stirring overnight, then 0.1 mL of the liquid phase was diluted to 0.25 mg/mL and filtered with 0.2 μm syringe filters. The data was analyzed with the Cirrus GPC Software 3.2.

3. Results and discussion

3.1. Coagulated and thermostabilized cellulose films

Cellulose in its native state is composed of at least two crystalline polymorphs, cellulose Iα and Iβ. Wang et al. proposed up to 7 different forms in the primary cell wall [67]. ^{13}C solid state CP NMR is a powerful tool to determine different cellulose polymorphs by distinguishing between the well-defined chemical shift pattern of crystalline and amorphous parts of cellulose.

The cellulose pulp used as starting material contained cellulose I, amorphous cellulose and minor amounts of hemicellulose. Its ^{13}C solid state CP NMR spectrum shows multiple peaks at 105 ppm, assigned to the C1 carbon region, indicating the presence of cellulose I (Fig. 2a, blue) [68]. Multiple peaks were also observed for the region around 89 ppm corresponding to the crystalline cellulose carbon C4 region. The amorphous C4 region is characterized by a broader shoulder at around 84 ppm. The C2, C3 and C5 carbons appear between 70 and 80 ppm. The main peak at around 65 ppm belongs to the crystalline cellulose I and the broad shoulder at around 63 ppm to amorphous cellulose of the C6 carbon region. The peak observed at around 97 ppm is assignable to hemicellulose impurities [69].

The production of man-made fibers requires the dissolution of cellulose in an appropriate solvent prior to coagulation of cellulose. The ionic liquid [EMIM]OAc was chosen as solvent for our study since it has been widely used in literature to dissolve lignocellulosic materials [38,65,70] and in air-gap fiber spinning [27,28,71]. After dissolution and subsequent coagulation of dissolved pulp the original cellulose I is transformed into the more stable form, cellulose II [72] with varying amounts of amorphous regions. It has been shown that the solvent used to dissolve cellulose and the anti-solvent used for coagulation impact the crystallinity of the cellulose [30]. Here we chose two anti-solvents,

Table 2
Weight loss due to the thermostabilization at 245 °C of the coagulated films in H_2O or EtOH. LMW refers to low molecular weight lignin and HMW to high molecular weight lignin.

Sample	Coagulated and dried film (g)	Thermostabilized film at 245 °C (g)	Weight loss (g; %)
Cellulose in H_2O	0.23	0.21	0.02; 8.7
Cellulose in EtOH	0.15	0.11	0.04; 26.7
Cellulose LMW in H_2O	0.30	0.24	0.06; 20.0
Cellulose LMW in EtOH	0.22	0.17	0.05; 22.7
Cellulose HMW in H_2O	0.28	0.18	0.10; 35.7
Cellulose HMW in EtOH	0.24	0.14	0.10; 41.7

water (H_2O) and ethanol (EtOH).

Upon coagulation and mild drying, the signal intensity of the crystalline region of the C4 and C6 carbons are significantly reduced (Fig. 2). For the anti-solvent EtOH, it appears that the cellulose I has become amorphous while for the anti-solvent H_2O, distinctive peaks at approximately 107, 88.6 and 87.5 ppm emerge in the spectrum, indicating the presence of crystalline polymorph cellulose II [73]. Hence, when H_2O is used as an anti-solvent, the coagulated cellulose film shows some degree of crystallinity compared to cellulose coagulated in EtOH. The enhanced formation of crystalline regions during coagulation in the presence of water has been previously reported [38] and is attributed to a higher solubility of [EMIM]OAc in water, which could be beneficial for the formation of cellulose II.

To prepare CFs from cellulose or cellulose-lignin precursors and increase the char yield, thermostabilization below a temperature of approximately 300 °C is necessary. This step is required to mitigate losses due to volatilization of cellulose mainly over levoglucosan expulsion, which become significant at temperatures over 300 °C [31]. Thermostabilization reactions are commonly associated with the dehydration of cellulose. The operative mechanisms are still controversially discussed, however, recent findings by parts of our group suggest the formation of a polyfuranic network [41,47]. For thermostabilization up to 250 °C, which did not result in significant dehydration of cellulose, the formation of levoglucosan-end capped structures and crosslinked (poly)saccharides were evidenced [46]. The ^{13}C solid state CP NMR spectra of the thermostabilized cellulose films at 245 °C are shown in Fig. 2a. The formation of cellulose II during the coagulation with the anti-solvent H_2O has persisted the thermostabilization. Apart from cellulose II, the ^{13}C solid state CP NMR spectra appear very similar showing broad features of mainly amorphous cellulose. Studies have been performed on Kraft pulp and filter paper which reported on hornification and coalescence of the fibrils based on deconvolution of the C4 region according to extensive studies on these materials [40]. Unfortunately, the C4 region for coagulated cellulose which is present in this study is featureless and did not allow any further analysis.

We followed the solution NMR approach [46,63] and dissolved the coagulated and thermostabilized cellulose films in the electrolyte solution and recorded HSQCs (Fig. 2b). We observed the presence of xylan (marked with X) in the pulp which is not seen in the solid state NMR spectra. Indeed, the HSQCs showed evidence of levoglucosan end cap formation marked with L1-L5 which is not visible in the solid state NMR spectra most likely due to its low concentration. Interestingly, the HSQC for the thermostabilized cellulose films coagulated in the anti-solvent EtOH showed additional peaks highlighted with empty triangles, which could not be assigned but follow a similar chemical shift pattern as levoglucosan (Fig. 2b, black-blue). The peak at 4.25/79 ppm was also observed in a previous study but could not be clearly assigned [46]. In this study, albeit appearing only once, crosslinking was evident in

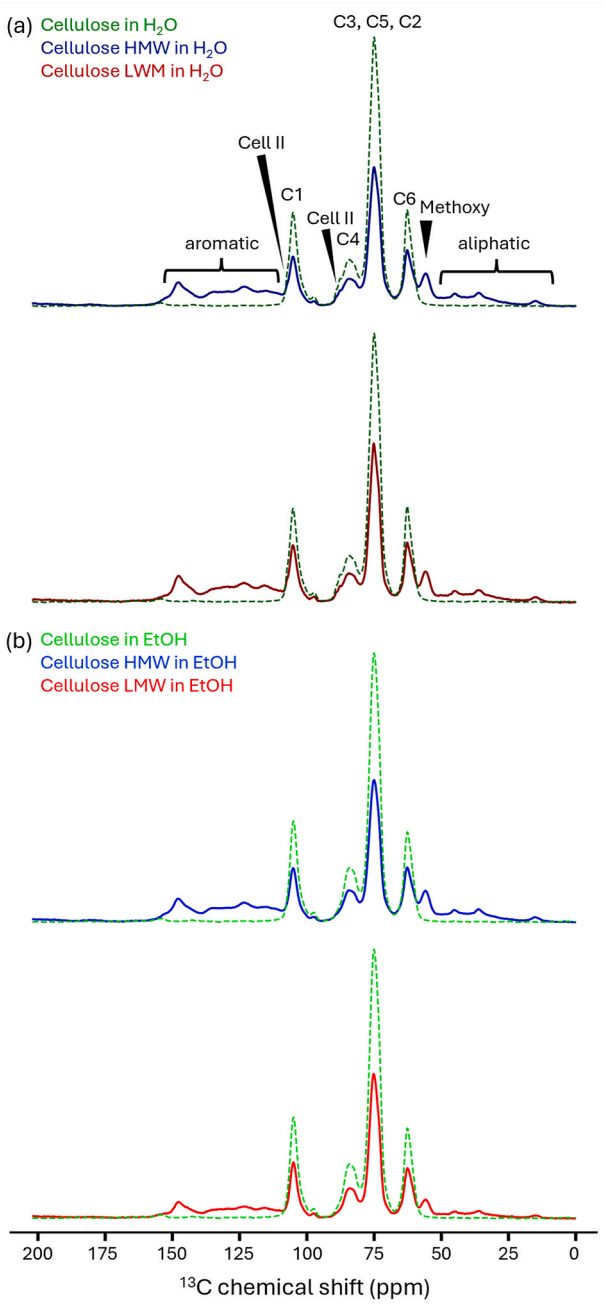

Fig. 3. ^{13}C CP solid state NMR spectra of cellulose and cellulose-lignin films coagulated in H_2O (a) and in EtOH (b). LMW refers to low molecular weight lignin, HMW to high molecular weight lignin, Cell I to cellulose I and Cell II to cellulose II.

complementarily conducted size exclusion chromatography measurements. Thus, it is likely connected with a moiety in a crosslinked polysaccharide structure. The weight decreases upon thermostabilization due to the formation of volatile gases such as CO_2, CO and H_2O (Table 2) and expulsion of low molecular weight tar fractions. The weight loss for cellulose coagulated in EtOH is higher (26.7 %) than for H_2O (8.7 %). This suggests a more pronounced degradation of the less crystalline sample.

3.2. Addition of lignin

Addition of lignin to bio-based CF precursors can increase the char yield. To obtain a suitable conversion, lignin leaching during the

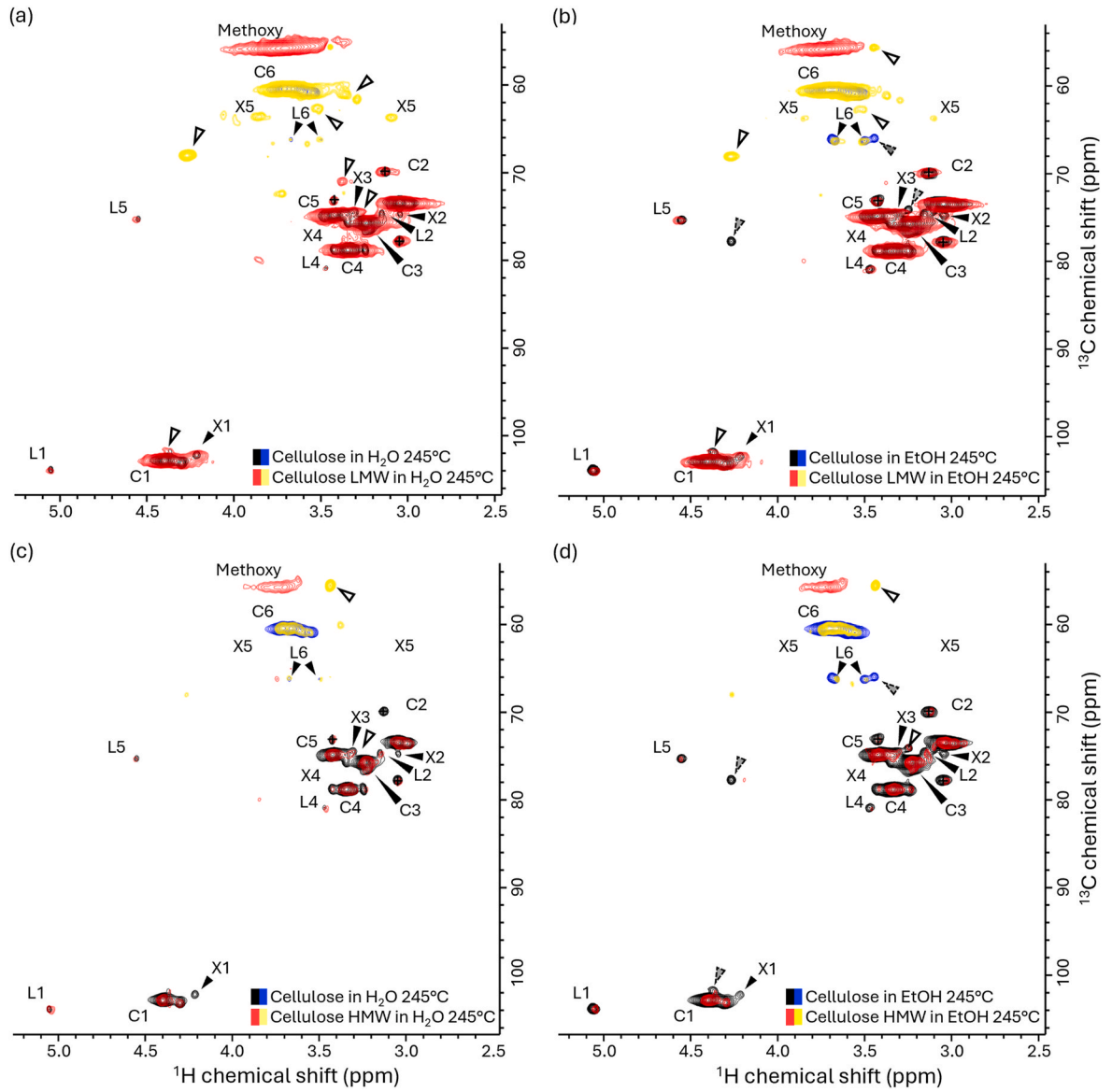

Fig. 4. 2D ^{1}H-^{13}C HSQC spectra of the coagulated (EtOH and H_2O) cellulose and cellulose-lignin films after thermostabilization at 245 °C. Open triangles identify unassigned peaks from unknown products, gray filled dashed triangles identify peaks that are present only in the coagulated cellulose samples and peaks marked with + are already present in the reference pulp. C refers to cellulose, X to xylan and L to levoglucosan end cap. The numbers refer to the atom number in the molecular structure. Blue and yellow are CH_2 groups while black and red are CH or CH_3 groups. A summary of the chemical shifts is presented in Table S2.

coagulation step should be minimized. To follow the impact of molecular weight, softwood Kraft lignin was fractionated into a low molecular (LMW, MW = 3.4 kDa) and a high molecular weight (HMW = 19 kDa) fraction. The size exclusion chromatogram is shown in Fig. S1 showing that two fractions were obtained after the fractionation (dashed blue and dashed red). The original distribution is shown in purple. The fractionation process is based on the solubility of lignin in different solvents which also implies that the fractions will have a different distribution of functional groups. Fig. S2 shows the HSQCs of the LMW and HMW lignin fraction showing common lignin side chains/linkages like A, B and C and the G-units which are mostly present in softwood lignin. It appears that the HMW fraction has a larger number of A linkages and a small fraction of xylan.

Fig. S1 shows in addition the molecular weight distribution of lignin in the coagulated films. In the coagulated cellulose HMW lignin, the molecular weight distribution of lignin is independent on the anti-solvent used. However, in the coagulated cellulose films with LMW lignin, the distribution shows some losses when EtOH is used as the anti-solvent compared to H_2O. This has also been confirmed visually as the coagulation bath turned brownish for EtOH and the low molecular weight system. Hence, we compared the HSQCs for lignin with the coagulated cellulose-lignin samples and could confirm that the main peaks of lignin are present (Fig. S3).

The corresponding ^{13}C solid state CP NMR spectra of the coagulated cellulose-lignin films are shown in Fig. 3. In comparison with the coagulated cellulose films, similar results about the formation of cellulose II were obtained for the cellulose-lignin blends when using H_2O as an anti-solvent. Additional peaks indicative of lignin were discerned, delineating distinct regions: an aromatic domain spanning 110–160 ppm, aliphatic groups within the range of 10–50 ppm, and methoxy groups located around approximately 56 ppm. To enable a simple comparison of the ^{13}C solid state CP NMR spectra which are not inherently quantitative, the recorded spectra were normalized by their total area. Some approaches were developed to estimate the lignin content in biomass [74] or the degree of polymerization of hydrolyzed cellulose [69] using solid state NMR but our focus has been on the reaction

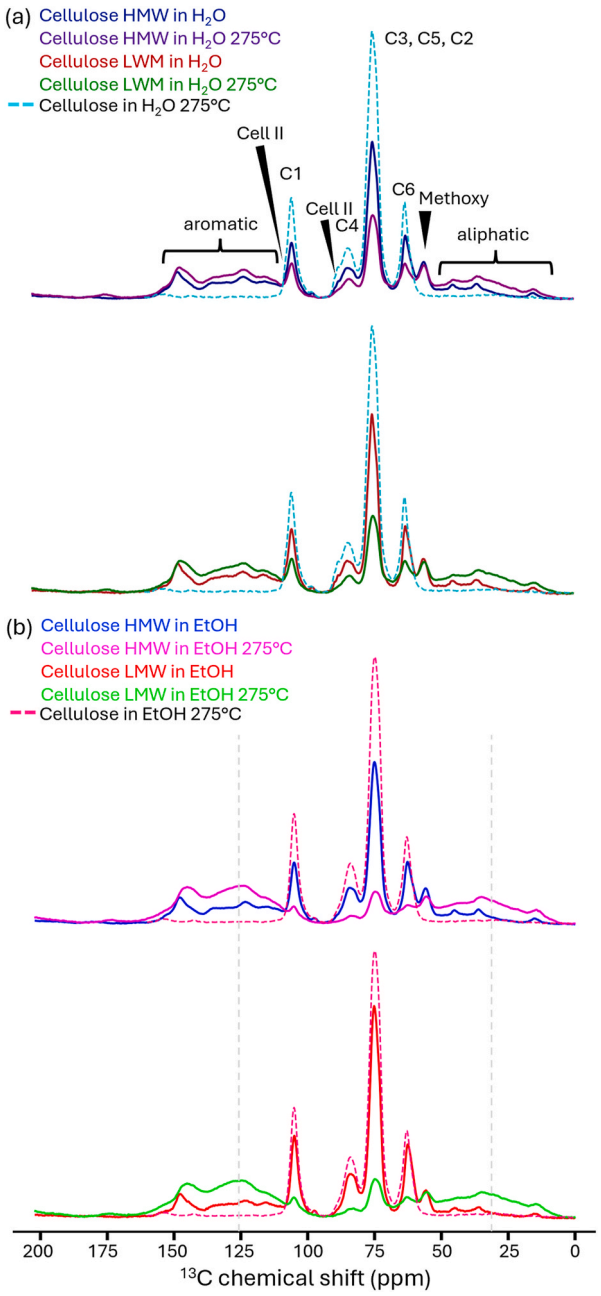

Fig. 5. ^{13}C solid state CP NMR on dried cellulose and cellulose-lignin films coagulated in H_2O and EtOH thermostabilized at 275 °C. Changes previously assigned to formation of carbonization intermediates highlighted with gray dashed line.

products and changes occurring during thermostabilization.

The ^{13}C CP/MAS spectrum of the coagulated cellulose-lignin LMW film in ethanol exhibits the lowest signal intensity in the lignin regions and the highest for the cellulose regions. This observation aligns with the expectation that the LMW lignin fraction is more soluble in ethanol, suggesting a higher likelihood of lignin leaching during the coagulation process which agrees with the size exclusion chromatography results. Consequently, the use of LMW lignin and ethanol as an anti-solvent both contribute to increased lignin leaching, resulting in a lesser amount of lignin remaining in the coagulated sample. Notably, the peak pattern of the LMW and the HMW lignin left in the cellulose films are very similar.

In order to follow the reaction products upon thermostabilization at 245 °C, 2D solution NMR is used again and the HSQCs are shown in Fig. 4. The formation of levoglucosan end caps and the presence of xylan were observed for all combinations, H_2O or EtOH and LMW or HMW. Most of the lignin peaks are not visible except the methoxy peak and the G-units (part of the spectra not shown) suggesting that the side chain groups might have reacted. For the anti-solvent H_2O and LMW lignin, there are new unassigned peaks marked with an empty triangle, which do neither overlap with the peaks from the thermostabilized cellulose nor the peaks from lignin (Fig. 4a). Similar unassigned peaks were also found for the anti-solvent EtOH and LMW lignin. For the HMW lignin, the HSQC spectra match the HSQC spectra of the coagulated cellulose without the addition of lignin expect for the anti-solvent EtOH, for which the unassigned peaks close to L5 and L6 highlighted with a gray filled dashed triangle are not visible. Hence, the addition of lignin seems to impact the reaction pathways for the anti-solvent EtOH. Interestingly, the weight loss was more pronounced for the anti-solvent EtOH compared for H_2O and the EtOH/HMW combination showed the biggest loss.

After thermostabilization at 275 °C, a large fraction of the samples became insoluble in the NMR electrolyte (Table 1) and the interpretation of solution NMR became challenging. However, solid state NMR showed to be more useful and the ^{13}C solid state CP NMR are shown in Fig. 5. In contrast to the coagulated and thermostabilized (275 °C) cellulose samples, the ^{13}C solid state CP NMR spectra of the coagulated and thermostabilized cellulose-lignin samples appeared different. There is a clear separation between the samples coagulated in H_2O and EtOH. When comparing lignin and cellulose intensities, there is an indication that more cellulose is present for the anti-solvent H_2O compared to EtOH. The EtOH samples lack cellulose II which still persists at 275 °C for the H_2O samples. The addition of lignin independently on the molecular weight in combination with the anti-solvent EtOH seems to catalyze the reaction rate. It could not be determined to which extend this observation is ascribable to either volatilization or initial carbonization reactions. However, the pattern of the aliphatic and aromatic region for the EtOH cellulose-lignin samples changed and showed broad peaks around 125 ppm and 30 ppm. This suggests the formation of other solid reaction products. Previous studies reported that a polyfuranic network serves as the major dehydration product formed at these temperatures, which exhibited peaks in similar spectral areas as observed herein. The peak around 30 ppm was assigned to aliphatic linkers present between different furanic moieties, which were associated with the band visible in the aromatic area [47]. The postulated structure for the dehydrated intermediates was based solely on their ^{13}C CP NMR spectra and their similarity to hydrochars investigated with solid state HETCOR experiments [75]. In a recent report the so-far not analytically accessible contribution of phenolic moieties to the broadened aromatic peak area in the 110–150 ppm range in the ^{13}C CP NMR spectra of dehydrated saccharides was highlighted [76]. Advanced hydroxyl-proton selection (HOPS) experiments could distinguish furans and phenols from one another in ^{13}C-enriched glucose-derived hydrochars [76].

In the present study, the observed broadened peaks in the aromatic and aliphatic regions are likewise attributable to dehydrated and condensed carbonization intermediates resulting from both cellulose dehydration and incorporated lignin structures (Fig. 5). With the applied experimental set-up further structural insights were, however, not accessible. Comparing the thermostabilization to 275 °C of cellulose alone with the cellulose-lignin blends a synergistic effect becomes apparent (Fig. 5). The cellulosic contributions diminish, while peaks in accordance with its dehydration intermediate become stronger. This effect is especially pronounced, if the formation of crystalline cellulose II moieties is prevented by using EtOH as an anti-solvent.

4. Conclusion

The impact of two different anti-solvents, H_2O and EtOH, and the addition of lignin on the coagulation and thermostabilization of cellulose-lignin blends were investigated using solid state and solution NMR. Solid state NMR proved to be useful for studying cellulose

polymorphs after coagulation and highlighted that the anti-solvent EtOH prevents the formation of cellulose II. This effect had an impact on subsequent thermostabilization reactions of cellulose-lignin blends, as evidenced by the earlier onset of dehydration reactions resulting in the formation of carbonization intermediates indicated by the solid state NMR spectra. On the other hand, solution NMR provided more insights in the chemical moieties present in the coagulated cellulose-lignin blends and the reactions occurring at lower thermostabilization temperatures. A better spectral resolution would be obtained by applying 2D solid state NMR. However, without the use of DNP or ^{13}C labeled material this would require unreasonable measurement time in comparison to a 3 hlong 2D solution NMR experiment. Hence the combination of both techniques is a promising way to understand influences of different coagulation conditions and elucidate reaction pathways occurring during thermostabilization. Our results showed that the anti-solvent impacted the reaction for cellulose only in the presence of lignin and its molecular weight fraction appeared to affect the formation of reaction products. Further studies will focus on elucidating the reaction of lignin during thermostabilization relevant to carbon fibers, batteries and supercapacitors research.

Declaration of competing interest

The authors declare that they have no known competing financial interests or personal relationships that could have appeared to influence the work reported in this paper.

Acknowledgements

DB, FG, JB and MH acknowledge funding from Tandem Forest via FORMAS (FR-2022/0002) and the Swedish NMR Centre for spectrometer time. LF and MH gratefully acknowledge funding from the Research Council of Finland (projects: 348354 and 353841) and financial support by the Foundation of Walter Ahlström. Dr. Tobias Sparrman is acknowledged for running the solid state NMR experiments.

Appendix A. Supplementary data

Supplementary data to this article can be found online at https://doi.org/10.1016/j.ssnmr.2024.101977.

Data availability

Data will be made available on request.

References

[1] W. Soon, S.L. Baliunas, A.B. Robinson, Z.W. Robinson, Environmental effects of increased atmospheric carbon dioxide, Clim. Res. 13 (1999) 149–164.
[2] S. Sharma, V. Sharma, S. Chatterjee, Contribution of plastic and microplastic to global climate change and their conjoining impacts on the environment - a review, Sci. Total Environ. 875 (2023) 162627.
[3] J.P. Tilsted, F. Bauer, C.D. Birkbeck, J. Skovgaard, J. Rootzén, Ending fossil-based growth: confronting the political economy of petrochemical plastics, One Earth 6 (2023) 607–619.
[4] G. Fiorentino, A. Zucaro, S. Ulgiati, Towards an energy efficient chemistry. Switching from fossil to bio-based products in a life cycle perspective, Energy 170 (2019) 720–729.
[5] A. Wazeer, A. Das, C. Abeykoon, A. Sinha, A. Karmakar, Composites for electric vehicles and automotive sector: a review, Green Energy Intell. Transp. 2 (2023) 100043.
[6] D.A. Baker, T.G. Rials, Recent advances in low-cost carbon fiber manufacture from lignin, J. Appl. Polym. Sci. 130 (2013) 713–728.
[7] T. Peijs, R. Kirschbaum, P.J. Lemstra, Chapter 5: a critical review of carbon fiber and related products from an industrial perspective, Adv. Ind. Eng. Polym. Res. 5 (2022) 90–106.
[8] J.F. Kadla, S. Kubo, R.A. Venditti, R.D. Gilbert, A.L. Compere, W. Griffith, Lignin-based carbon fibers for composite fiber applications, Carbon 40 (2002) 2913–2920.
[9] A.G. Dumanlı, A.H. Windle, Carbon fibres from cellulosic precursors: a review, J. Mater. Sci. 47 (2012) 4236–4250.
[10] X. Huang, Fabrication and properties of carbon fibers, Materials 2 (2009) 2369–2403.
[11] H. Mainka, O. Täger, E. Körner, L. Hilfert, S. Busse, F.T. Edelmann, A.S. Herrmann, Lignin – an alternative precursor for sustainable and cost-effective automotive carbon fiber, J. Mater. Res. Technol. 4 (2015) 283–296.
[12] A.A. Ogale, M. Zhang, J. Jin, Recent advances in carbon fibers derived from biobased precursors, J. Appl. Polym. Sci. 133 (2016).
[13] E. Sjöholm, C. Olsson, B. Hagström, A. Reimann, Carbon Fibres from Lignin-Cellulose Precursor, 2015.
[14] N. Byrne, R. De Silva, Y. Ma, H. Sixta, M. Hummel, Enhanced stabilization of cellulose-lignin hybrid filaments for carbon fiber production, Cellulose 25 (2018) 723–733.
[15] A. Bengtsson, J. Bengtsson, C. Olsson, M. Sedin, K. Jedvert, H. Theliander, E. Sjöholm, Improved yield of carbon fibres from cellulose and kraft lignin, Holzforschung 72 (2018) 1007–1016.
[16] N.-D. Le, M. Trogen, Y. Ma, R.J. Varley, M. Hummel, N. Byrne, Cellulose-lignin composite fibers as precursors for carbon fibers: Part 2 – the impact of precursor properties on carbon fibers, Carbohydr. Polym. 250 (2020) 116918.
[17] M. Trogen, N.-D. Le, D. Sawada, C. Guizani, T.V. Lourençon, L. Pitkänen, H. Sixta, R. Shah, H. O'Neill, M. Balakshin, N. Byrne, M. Hummel, Cellulose-lignin composite fibres as precursors for carbon fibres. Part 1 – manufacturing and properties of precursor fibres, Carbohydr. Polym. 252 (2021) 117133.
[18] P. Wannid, B. Hararak, S. Padee, W. Klinsukhon, N. Suwannamek, M. Raita, V. Champreda, C. Prahsarn, Fiber melt spinning and thermo-stabilization of para-rubber wood lignin: an approach for fully biomass precursor preparation, ACS Omega 8 (2023) 33891–33903.
[19] M. Zhang, A.A. Ogale, Carbon fibers from dry-spinning of acetylated softwood kraft lignin, Carbon 69 (2014) 626–629.
[20] C. Olsson, E. Sjöholm, A. Reimann, Carbon fibres from precursors produced by dry-jet wet-spinning of kraft lignin blended with kraft pulps, Holzforschung 71 (2017) 275–283.
[21] J. Bengtsson, K. Jedvert, T. Köhnke, H. Theliander, The challenge of predicting spinnability: investigating benefits of adding lignin to cellulose solutions in air-gap spinning, J. Appl. Polym. Sci. 138 (2021) 50629.
[22] L. Svenningsson, J. Bengtsson, K. Jedvert, W. Schlemmer, H. Theliander, L. Evenäs, Disassociated molecular orientation distributions of a composite cellulose–lignin carbon fiber precursor: a study by rotor synchronized NMR spectroscopy and X-ray scattering, Carbohydr. Polym. 254 (2021) 117293.
[23] E. Frank, L.M. Steudle, D. Ingildeev, J.M. Spörl, M.R. Buchmeiser, Carbon fibers: precursor systems, processing, structure, and properties, Angew. Chem., Int. Ed. Engl. 53 (2014) 5262–5298.
[24] A. Lehmann, H. Ebeling, H.-P. Fink, Method for the Production of Lignin-Containing Precursor Fibres and Also Carbon Fibres, 2012.
[25] Y. Ma, S. Asaadi, L.-S. Johansson, P. Ahvenainen, M. Reza, M. Alekhina, L. Rautkari, A. Michud, L. Hauru, M. Hummel, H. Sixta, High-strength composite fibers from cellulose–lignin blends regenerated from ionic liquid solution, ChemSusChem 8 (2015) 4030–4039.
[26] R. Protz, A. Lehmann, J. Ganster, H.-P. Fink, Solubility and spinnability of cellulose-lignin blends in aqueous NMMO, Carbohydr. Polym. 251 (2021) 117027.
[27] A. Bengtsson, J. Bengtsson, M. Sedin, E. Sjöholm, Carbon fibers from lignin-cellulose precursors: effect of stabilization conditions, ACS Sustain. Chem. Eng. 7 (2019) 8440–8448.
[28] J. Bengtsson, K. Jedvert, A. Hedlund, T. Köhnke, H. Theliander, Mass transport and yield during spinning of lignin-cellulose carbon fiber precursors, Holzforschung 73 (2019) 509–516.
[29] X. Cao, X. Peng, S. Sun, L. Zhong, S. Wang, F. Lu, R. Sun, Impact of regeneration process on the crystalline structure and enzymatic hydrolysis of cellulose obtained from ionic liquid, Carbohydr. Polym. 111 (2014) 400–403.
[30] S. Naserifar, A. Koschella, T. Heinze, D. Bernin, M. Hasani, Investigation of cellulose dissolution in morpholinium-based solvents: impact of solvent structural features on cellulose dissolution, RSC Adv. 13 (2023) 18639–18650.
[31] Kawamoto H Review of reactions and molecular mechanisms in cellulose pyrolysis Curr. Org. Chem. 20 2444–2457.
[32] P.T. Larsson, K. Wickholm, T. Iversen, A CP/MAS13C NMR investigation of molecular ordering in celluloses, Carbohydr. Res. 302 (1997) 19–25.
[33] T. Liitiä, S.L. Maunu, B. Hortling, Solid State NMR Studies on Cellulose Crystallinity in Fines and Bulk Fibres Separated from Refined Kraft Pulp, vol. 54, 2000, 618–24.
[34] H. Kono, S. Yunoki, T. Shikano, M. Fujiwara, T. Erata, M. Takai, CP/MAS 13C NMR study of cellulose and cellulose derivatives. 1. Complete assignment of the CP/MAS 13C NMR spectrum of the native cellulose, J. Am. Chem. Soc. 124 (2002) 7506–7511.
[35] D.L. VanderHart, R.H. Atalla, Studies of microstructure in native celluloses using solid-state carbon-13 NMR, Macromolecules 17 (1984) 1465–1472.
[36] R.H. Atalla, J.C. Gast, D.W. Sindorf, V.J. Bartuska, G.E. Maciel, Carbon-13 NMR spectra of cellulose polymorphs, J. Am. Chem. Soc. 102 (1980) 3249–3251.
[37] J.F. Haw, G.E. Maciel, H.A. Schroeder, Carbon-13 nuclear magnetic resonance spectrometric study of wood and wood pulping with cross polarization and magic-angle spinning, Anal. Chem. 56 (1984) 1323–1329.
[38] Å. Östlund, A. Idström, C. Olsson, P.T. Larsson, L. Nordstierna, Modification of crystallinity and pore size distribution in coagulated cellulose films, Cellulose 20 (2013) 1657–1667.
[39] M. Foston, Advances in solid-state NMR of cellulose, Curr. Opin. Biotechnol. 27 (2014) 176–184.
[40] P. Jusner, M. Bacher, J. Simon, F. Bausch, H. Khaliliyan, S. Schiehser, I. Sumerskii, E. Schwaiger, A. Potthast, T. Rosenau, Analyzing the effects of thermal stress on insulator papers by solid-state 13C NMR spectroscopy, Cellulose 29 (2022) 1081–1095.

[41] I. Pastorova, R.E. Botto, P.W. Arisz, J.J. Boon, Cellulose char structure: a combined analytical Py-GC-MS, FTIR, and NMR study, Carbohydr. Res. 262 (1994) 27–47.
[42] J. Zawadzki, M. Wisniewski, 13C NMR study of cellulose thermal treatment, J. Anal. Appl. Pyrolysis 62 (2002) 111–121.
[43] Y. Sekiguchi, J.S. Frye, F. Shafizadeh, Structure and formation of cellulosic chars, J. Appl. Polym. Sci. 28 (1983) 3513–3525.
[44] H. Knicker, M. Velasco-Molina, M. Knicker, 2D solid-state HETCOR 1H-13C NMR experiments with variable cross polarization times as a tool for a better understanding of the chemistry of cellulose-based pyrochars—a tutorial, Appl. Sci. 11 (2021) 8569.
[45] M. Jang, L. Fliri, M. Trogen, D. Choi, J.-H. Han, J. Kim, S.-K. Kim, S. Lee, S.-S. Kim, M. Hummel, Accelerated thermostabilization through electron-beam irradiation for the preparation of cellulose-derived carbon fibers, Carbon 218 (2024) 118759.
[46] L. Fliri, C. Guizani, I.Y. Miranda-Valdez, L. Pitkänen, M. Hummel, Reinvestigating the concurring reactions in early-stage cellulose pyrolysis by solution state NMR spectroscopy, J. Anal. Appl. Pyrolysis 175 (2023) 106153.
[47] L. Fliri, K. Dubivka, D. Rusakov, A. Volikov, C. Guizani, S. Hietala, S. Filonenko, M. Hummel, Identification of a polyfuran network as the initial carbonization intermediate in cellulose pyrolysis: a comparative analysis with cellulosic hydrochars, J. Anal. Appl. Pyrolysis 181 (2024) 106591.
[48] R.H. Newman, L.M. Davies, P.J. Harris, Solid-state 13C nuclear magnetic resonance characterization of cellulose in the cell walls of Arabidopsis thaliana leaves, Plant Physiol. 111 (1996) 475–485.
[49] G. Zuckerstätter, G. Schild, P. Wollboldt, T. Röder, H. Weber, H. Sixta, The elucidation of cellulose supramolecular structure by 13C CP-MAS NMR, Lenzing. Berichte 87 (2009).
[50] A. Idström, S. Schantz, J. Sundberg, B.F. Chmelka, P. Gatenholm, L. Nordstierna, 13C NMR assignments of regenerated cellulose from solid-state 2D NMR spectroscopy, Carbohydr. Polym. 151 (2016) 480–487.
[51] T. Sparrman, L. Svenningsson, K. Sahlin-Sjövold, L. Nordstierna, G. Westman, D. Bernin, A revised solid-state NMR method to assess the crystallinity of cellulose, Cellulose 26 (2019) 8993–9003.
[52] A. Kumar, H. Durand, E. Zeno, C. Balsollier, B. Watbled, C. Sillard, S. Fort, I. Baussanne, N. Belgacem, D. Lee, S. Hediger, M. Demeunynck, J. Bras, G.D. Paëpe, The surface chemistry of a nanocellulose drug carrier unravelled by MAS-DNP, Chem. Sci. 11 (2020) 3868–3877.
[53] W. Zhao, A. Kirui, F. Deligey, F. Mentink-Vigier, Y. Zhou, B. Zhang, T. Wang, Solid-state NMR of unlabeled plant cell walls: high-resolution structural analysis without isotopic enrichment, Biotechnol. Biofuels 14 (2021) 14.
[54] T. Wang, Y.B. Park, M.A. Caporini, M. Rosay, L. Zhong, D.J. Cosgrove, M. Hong, Sensitivity-enhanced solid-state NMR detection of expansin's target in plant cell walls, Proc. Natl. Acad. Sci. USA 110 (2013) 16444–16449.
[55] A. Chakraborty, F. Deligey, J. Quach, F. Mentink-Vigier, P. Wang, T. Wang, Biomolecular complex viewed by dynamic nuclear polarization solid-state NMR spectroscopy, Biochem. Soc. Trans. 48 (2020) 1089–1099.
[56] R. Evans, R.H. Newman, U.C. Roick, I.D. Suckling, A.F.A. Wallis, Changes in cellulose crystallinity during kraft pulping, Comparison of Infrared, X-ray Diffraction and Solid State NMR Results 49 (1995) 498–504.
[57] K. Schenzel, S. Fischer, E. Brendler, New method for determining the degree of cellulose I crystallinity by means of FT Raman spectroscopy, Cellulose 12 (2005) 223–231.
[58] S. Park, D.K. Johnson, C.I. Ishizawa, P.A. Parilla, M.F. Davis, Measuring the crystallinity index of cellulose by solid state 13C nuclear magnetic resonance, Cellulose 16 (2009) 641–647.
[59] P. Ahvenainen, I. Kontro, K. Svedström, Comparison of sample crystallinity determination methods by X-ray diffraction for challenging cellulose I materials, Cellulose 23 (2016) 1073–1086.
[60] J.-L. Wen, S.-L. Sun, B.-L. Xue, R.-C. Sun, Recent advances in characterization of lignin polymer by solution-state nuclear magnetic resonance (NMR) methodology, Materials 6 (2013) 359–391.
[61] P. Korntner, I. Sumerskii, M. Bacher, T. Rosenau, A. Potthast, Characterization of technical lignins by NMR spectroscopy: optimization of functional group analysis by 31P NMR spectroscopy, Holzforschung 69 (2015) 807–814.
[62] Y. Lu, Y.-C. Lu, H.-Q. Hu, F.-J. Xie, X.-Y. Wei, X. Fan, Structural characterization of lignin and its degradation products with spectroscopic methods, J. Spectrosc. 2017 (2017) 8951658.
[63] L. Fliri, K. Heise, T. Koso, A.R. Todorov, D.R. Del Cerro, S. Hietala, J. Fiskari, I. Kilpeläinen, M. Hummel, A.W.T. King, Solution-state nuclear magnetic resonance spectroscopy of crystalline cellulosic materials using a direct dissolution ionic liquid electrolyte, Nat. Protoc. 18 (2023) 2084–2123.
[64] C. Cui, R. Sun, D.S. Argyropoulos, Fractional precipitation of softwood kraft lignin: isolation of narrow fractions common to a variety of lignins, ACS Sustain. Chem. Eng. 2 (2014) 959–968.
[65] A. Hedlund, T. Köhnke, H. Theliander, Diffusion in ionic liquid–cellulose solutions during coagulation in water: mass transport and coagulation rate measurements, Macromolecules 50 (2017) 8707–8719.
[66] T. Bräuniger, P. Wormald, P. Hodgkinson, Improved Proton Decoupling in NMR Spectroscopy of Crystalline Solids Using the Spinal-64 Sequence *Current Developments In Solid State NMR Spectroscopy* Ed N Müller and P K Madhu, Springer, Vienna, 2003, pp. 69–74.
[67] T. Wang, H. Yang, J.D. Kubicki, M. Hong, Cellulose structural polymorphism in plant primary cell walls investigated by high-field 2D solid-state NMR spectroscopy and density functional theory calculations, Biomacromolecules 17 (2016) 2210–2222.
[68] D.H. Brouwer, J.G Mikolajewski, Resolving the discrepancies in reported 13C solid state NMR chemical shifts for native celluloses, Cellulose 30 (2023) 4827–4839.
[69] S. Yuan, M.V. Tyufekchiev, M.T. Timko, K. Schmidt-Rohr, Direct quantification of the degree of polymerization of hydrolyzed cellulose by solid-state NMR spectroscopy, Cellulose 29 (2022) 2131–2144.
[70] A. Hedlund, T. Köhnke, J. Hagman, U. Olsson, H. Theliander, Microstructures of cellulose coagulated in water and alcohols from 1-ethyl-3-methylimidazolium acetate: contrasting coagulation mechanisms, Cellulose 26 (2019) 1545–1563.
[71] J. Bengtsson, K. Jedvert, T. Köhnke, H. Theliander, Identifying breach mechanism during air-gap spinning of lignin–cellulose ionic-liquid solutions, J. Appl. Polym. Sci. 136 (2019) 47800.
[72] R.L. Dudley, C.A. Fyfe, P.J. Stephenson, Y. Deslandes, G.K. Hamer, R. H. Marchessault, High-resolution carbon-13 CP/MAS NMR spectra of solid cellulose oligomers and the structure of cellulose II, J. Am. Chem. Soc. 105 (1983) 2469–2472.
[73] G. Zuckerstätter, N. Terinte, H. Sixta, K.C. Schuster, Novel insight into cellulose supramolecular structure through 13C CP-MAS NMR spectroscopy and paramagnetic relaxation enhancement, Carbohydr. Polym. 93 (2013) 122–128.
[74] D.F. Cipriano, L.S. Chinelatto, S.A. Nascimento, C.A. Rezende, S.M.C. De Menezes, J.C.C. Freitas, Potential and limitations of 13C CP/MAS NMR spectroscopy to determine the lignin content of lignocellulosic feedstock, Biomass Bioenergy 142 (2020) 105792.
[75] I van Zandvoort, E.J. Koers, M. Weingarth, P.C.A. Bruijnincx, M. Baldus, B. M. Weckhuysen, Structural characterization of 13C-enriched humins and alkali-treated 13C humins by 2D solid-state NMR, Green Chem. 17 (2015) 4383–4392.
[76] S. Yuan, A. Brown, Z. Zheng, R.L. Johnson, K. Agro, A. Kruse, M.T. Timko, K. Schmidt-Rohr, Glucose hydrochar consists of linked phenol, furan, arene, alkyl, and ketone structures revealed by advanced solid-state nuclear magnetic resonance, Solid State Nucl. Magn. Reson. 134 (2024) 101973.